Preprints (www.preprints.org) | NOT PEER-REVIEWED | Posted: 11 October 2021

doi:10.20944/preprints202110.0169.v1

Article

Hydro-thermal modeling for geothermal energy extraction from Soultz-sous-Forêts, France

Saeed Mahmoodpour[1*], Mrityunjay Singh[2], Aysegul Turan[3], Kristian Bär[4], and Ingo Sass[5,6]

[1] Group of Geothermal Science and Technology, Institute of Applied Geosciences, Technische Universität Darmstadt; saeed.mahmoodpour@tu-darmstadt.de
[2] Group of Geothermal Science and Technology, Institute of Applied Geosciences, Technische Universität Darmstadt; mrityunjay.singh@tu-darmstadt.de
[3] Group of Geothermal Science and Technology, Institute of Applied Geosciences, Technische Universität Darmstadt; turan@geo.tu-darmstadt.de
[4] Group of Geothermal Science and Technology, Institute of Applied Geosciences, Technische Universität Darmstadt; baer@geo.tu-darmstadt.de
[5] Group of Geothermal Science and Technology, Institute of Applied Geosciences, Technische Universität Darmstadt;
[6] Darmstadt Graduate School of Excellence Energy Science and Engineering, Technische Universität Darmstadt; sass@geo.tu-darmstadt.de

* Correspondence: Saeed: saeed.mahmoodpour@tu-darmstadt.de; Mrityunjay: mrityunjay.singh@tu-darmstadt.de

Abstract: The deep geothermal industrial project at Soultz-sous-Forêts is located in the Upper Rhine Graben, France. As part of the MEET project, this study aims to evaluate the possibility of extracting higher amounts of energy from the existing industrial infrastructure. To achieve this objective, the effect of reinjecting fluid at lower temperature than the current fluid injection temperature of 70 °C was modelled and the drop in the production wellhead temperature for 100 years of operation was quantified. Two injection-production rate scenarios were considered and compared for their effect on overall production wellhead temperature. For each scenario, reinjection temperatures of 40 °C, 50 °C and 60 °C were chosen and compared with the 70 °C injection case. For the lower production rate scenario, the results show that the production wellhead temperature is approximately 1-1.5 °C higher than for the higher production rate scenario after 100 years of operation. In conclusion, no significant thermal breakthrough has been observed with the applied flow rates and lowered injection temperatures even after 100 years of operation.

Keywords: Soultz-sous-Forêts, EGS, Hydro-thermal modeling, Wellbore coupling

1. Introduction

Geothermal energy is a clean, renewable and low-cost solution for heating and power generation. One of the most challenging problems that humanity is facing is how to mitigate the climate change and anthropogenic emission of carbon dioxide, in order to achieve the Paris agreement that limits the atmospheric temperature rise to 2 °C or less [1]. Carbon geosequestration is the most desirable solution to this problem [2-5]. However associated cost and underdeveloped technology limits the industry from its implementation. Therefore, use of geothermal energy to replace the carbon-based energy sources is gaining momentum [6]. A milestone of 2 million of heat pumps installation by the European geothermal heat pump market was achieved in the year 2019 [7]. The geothermal heat usage and electricity production in Europe is expected to grow up to 880-1050 TWh/year and 100-210 TWh/yr in 2050 respectively. This contribution is equivalent to 4-7% of European power generation in the year 2050 [8]. As part of MEET project, a numerical hydrothermal

© 2021 by the author(s). Distributed under a Creative Commons CC BY license.

Preprints (www.preprints.org) | NOT PEER-REVIEWED | Posted: 11 October 2021 doi:10.20944/preprints202110.0169.v1

model was developed to critically validate the flow behavior of Soultz-sous-Forêts geothermal power plant from existing operational data. Furthermore, our model was enhanced by including discrete fault structures and validated with operational data to allow for a realistic prediction of the future operational behavior.

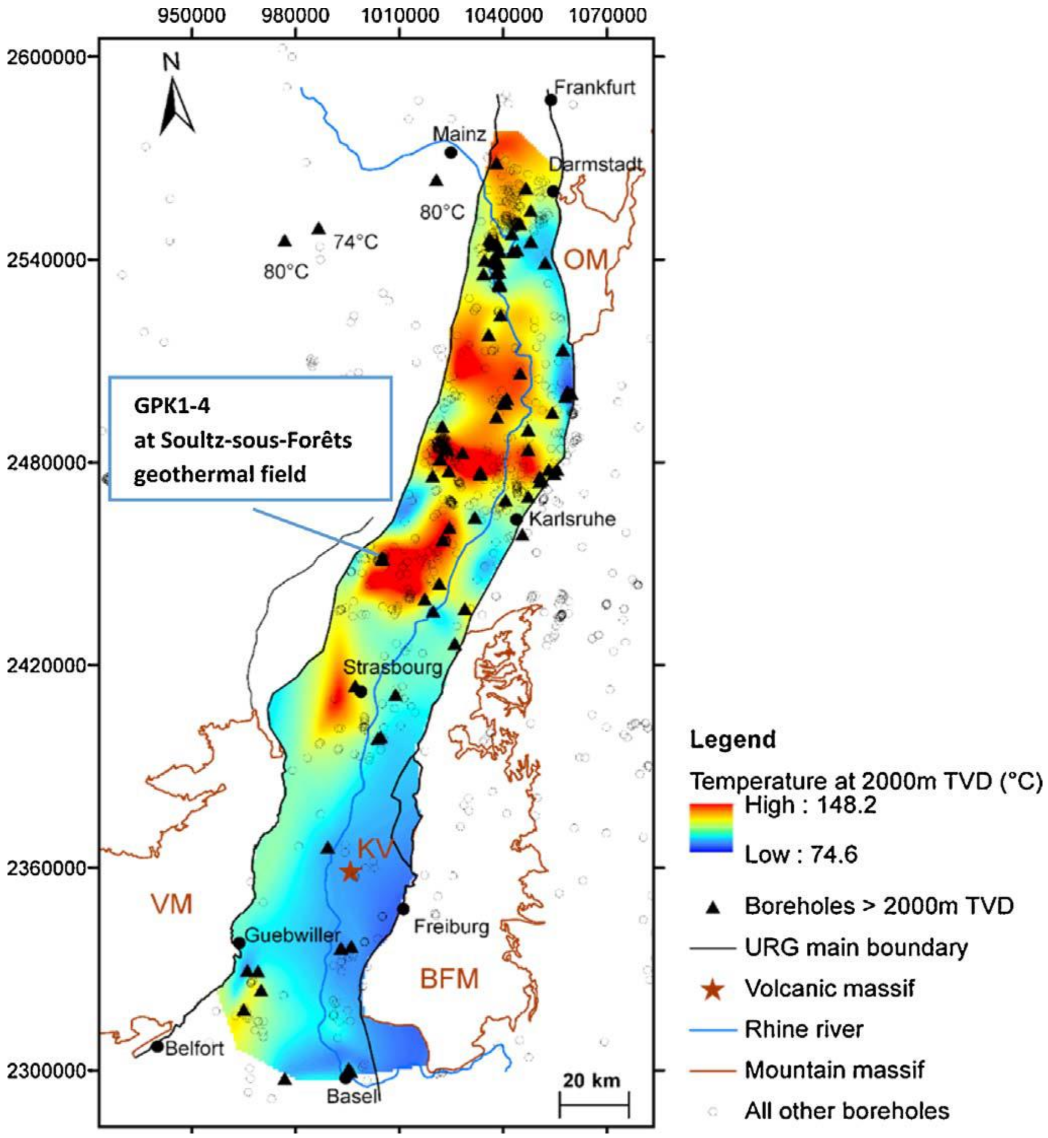

Figure 1: Temperature distribution at 2 km depth TVD in the Upper Rhine Graben [9].

Table 1: Rock matrix parameters [10]

Parameter	Unit	Upper sediment	Buntsandstein	Granite
Hydraulic conductivity	m s^{-1}	5×10^{-8}	1×10^{-8}	9×10^{-9}
Specific storage	1 m^{-1}	8×10^{-7}	5×10^{-7}	1.75×10^{-8}
Porosity	-	0.1	0.03	0.03
Thermal conductivity	W m^{-1} K^{-1}	2.8	2.5	2.5
Thermal capacity	J m^{-3} K^{-1} ·	2×10^{6}	3.2×10^{6}	2.9×10^{6}
Heat production	W m^{-3}	5×10^{-7}	5×10^{-7}	3×10^{-7}

Preprints (www.preprints.org) | NOT PEER-REVIEWED | Posted: 11 October 2021 doi:10.20944/preprints202110.0169.v1

Soultz-sous-Forêts is located in the central Upper Rhine Graben, France and has a great potential for the geothermal energy exploitation. Soultz-sous-Forêts is the most investigated site in terms of geoscientific studies. The top 1.5 km of the geological succession is made of thick Quaternary and Tertiary sediments, Mesozoic to Paleozoic sedimentary rocks above the crystalline basement which is represented by naturally fractured granite (See Figure 1). The Mesozoic to Paleozoic sedimentary rocks can be subdivided into two layers: Buntsandstein and Permian. The Buntsandstein is approximately 350 m thick and comprised of fluvial deposits while the Permian represents more alluvial continental deposit filling the paleo-basin of the variscan orogeny [11]. The basement is composed of monzogranite with K-feldspar mega crystals with localized concentration of biotite (Depth between 1420 m to 4700 m) and a two-mica granite containing muscovite (Depth between 4700 m to 5000 m) [12; 13]. In Table 1, the rock properties for the two sandstone layers and granite are listed [10; 14]. The sedimentary section has a maximum geothermal gradient of up to >100 K km^{-1} making the Soultz-sous-Forêts site ideal for geothermal energy extraction [15]. Free convection along the major faults [16; 17; 18] are the primary reason causing the increased thermal gradients. For depth greater than 3,700 m, geothermal gradient becomes 10 K/km. Figure 2 shows the geothermal gradient at the Soultz-sous-Forêts site. Sausse et al. [19] and Dezayes et al. [20] used borehole image logs and core studies to characterize 3D realistic and static fractures of Soultz granite. Sausse et al. [19] found 53 structures including 39 fracture zones, 7 microseismic structures and 6 vertical seismic profiling (VSP) at the Soultz-sous-Forêts site. At the same time, Dezayes et al. [20] also identified 39 fractures aligned with a general strike of N160^{O}E at Soultz site. The sedimentary layer above 1,400 m is considered for geothermal activity in the literature due to their remoteness from the main fluid circulation, and they are considered as a caprock.

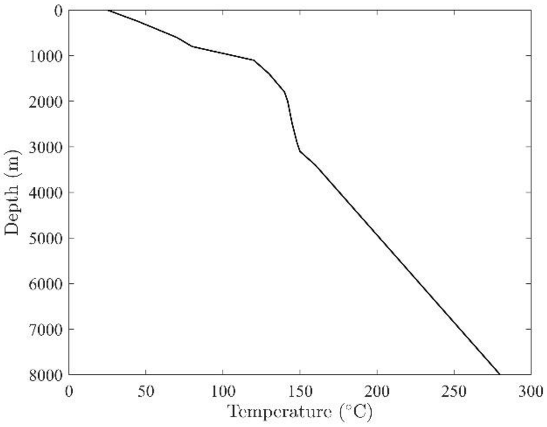

Figure 2: Geothermal gradient at the Soultz-sous-Forêts site. Here anomaly in temperature is observable in the top 3 km section or in the sedimentary layer. We assumed 10 ℃ temperature at the surface to calculate this geothermal gradient [Rolin:18].

The geothermal project was commenced at Soultz-sous-Forêts in year 1984 and the drilling started in year 1987 [21]. The earliest plan was to create a fractured granite reservoir in the deep crystalline rock at a depth of 5 km to generate electricity. The industrial electricity production at this site started in June 2016. Presently, the Soultz-sous-Forêts site operates three wells with a maximum depth of up to 5000 m (GPK-2, GPK-3 and GPK-4, see Figure 3). These wells follow the main fault along the NNW-SSE direction. The binary geothermal power plant is working on an Organic Rankine Cycle (ORC) for the heat to electricity conversion. The production well is GPK-2 while two wells GPK-3 and GPK-4 are re-injection wells. The hot fluid produced from GPK-2 is fed-into the heat exchanger

Preprints (www.preprints.org) | NOT PEER-REVIEWED | Posted: 11 October 2021

doi:10.20944/preprints202110.0169.v1

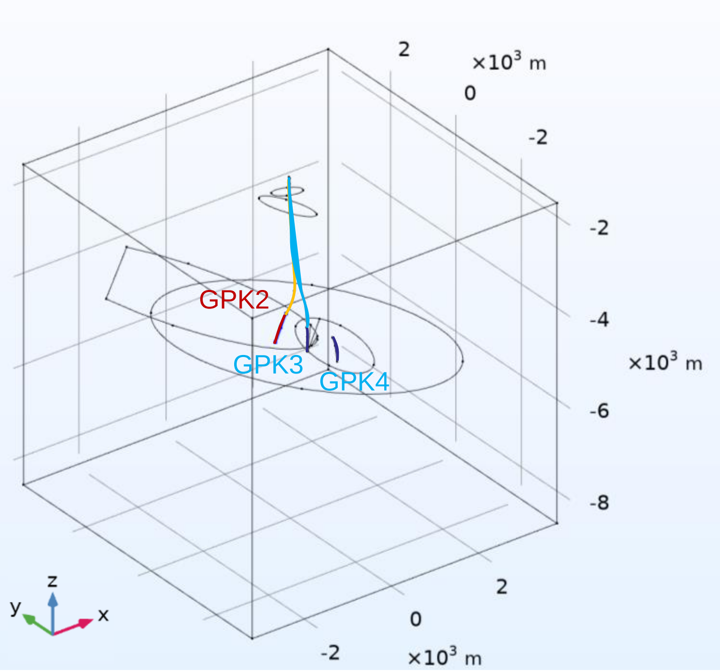

Figure 3: Geometry for numerical modeling of Soultz-sous-Forêts geothermal site.

where the heat is transferred to the isobutane of the ORC cycle and reinjected after being cooled. The fluid production temperature at the Soultz plant is >150 °C and the injection temperature is 70 °C. The production well (GPK-2), and one injection well (GPK-3) indicate fluid leakage, in the respective depth intervals between 1431 m – 4170 m measured depth from ground level (MDGL)) and 1447 m – 3988 m MDGL), respectively [22]. Both injection wells are cased only at the top while the granitic reservoir section is not completed and in open-hole condition.

For the model geometry, only the hydraulically active fractures with high permeability, as proven by thermal anomalies, detected microseismicity during stimulation and operation [19] and which are intersecting multiple wells were included. The model is thus limited to only 5 major fractures or fault zones as shown in Figure 3. The properties of these fractures (fault zones) are listed in Table 2.

Although the Soultz-sous-Forêts site has been the focus of more than 60 PhD theses and 300 peer reviewed articles [10], only a few hydrothermal modelling studies were conducted to understand the hydro-thermal behavior of the reservoir in detail over the last years. These studies were coupled with and validated by field operational data specifically with tracer tests to understand the flow path within the fractured granite [14].

The flow circulation between GPK-3 and GPK-2 wells was addressed by Sanjuan et al. [22] through an analytical dispersive transfer model whereas Blumenthal et al. [23], Gessner et al. [24] and Egert et al. [25] also used dispersive transport models for Soultz-sous-Forêts site. They investigated the hydraulic connectivity between the injection well (GPK3) and production well (GPK2 and GPK4) using a multi-well tracer test. Gentier et al. [26] developed the first discrete fracture network (DFN) model while employing a particle tracking method to consider the hydraulically active parts and fracture sets for both wells.

More recent modelling studies include Magnenet et al. [27], where a 2D THM model was developed based on a finite element grid (FEM), Aliyu and Chen [28], where finite element method (FEM) was used to model hydro-thermal (HT) processes of Soultz while using different working fluids, and most recently Vallier et al. [14], where a THM model based on FEM was developed at reservoir scale coupled with gravity measurements.

Previous studies showed that a single-fracture approach is not sufficient to represent the hydraulic flow existing at Soultz and 2D models are limited to represent the site in terms of the complex geometry and interconnection of dominating faults. Thus, this study takes its roots from the developed 3D THM model based on FEM while hosting 5 fractures (FZ1800, FZ2120, FZ4760, FZ4770, FZ4925, also see table 2) [10].

From the above literature, it is clear that cold water is injected at 70 ℃ through both the injection wells. Therefore, injection of cold water below this temperature may enable much higher geothermal energy extraction. However, there are no numerical studies so far to support this idea. In the presented study here, the energy extraction potential from Soultz-Sous-Forêts for 100 years is investigated and the thermal drawdown at the production well can be quantified. The manuscript outline is as follow: first it presents a brief geological setting of Soultz-Sous-Forêts, followed by numerical modeling studies for the site. Furthermore, the mathematical and computational technique to model hydro-thermal processes during heat mining from a fractured reservoir is discussed. Next, the wellbore-reservoir coupling is demonstrated and its impact on wellhead temperature is quantified. In the following section, model results and their discussion are followed by final conclusions.

Table 2: Fault parameters [10]

Parameter	Unit	FZ1800	FZ2120	FZ4760	FZ4770	FZ4925
Hydraulic conductivity	m s^{-1}	6.08×10^{-6}	1.7×10^{-5}	0.05	2×10^{-5}	6.3×10^{-5}
Specific storage	1 m^{-1}	2×10^{-6}	2×10^{-6}	2×10^{-6}	2×10^{-6}	2×10^{-6}
Porosity	-	0.1	0.1	0.1	0.1	0.1
Thermal conductivity	W m^{-1} K^{-1}	2.5	2.5	2.5	2.5	2.5
Thermal capacity	J m^{-3} K^{-1}	2.9×10^{-6}	2.9×10^{-6}	2.9×10^{-6}	2.9×10^{-6}	2.9×10^{-6}
Thickness	m	12	15	8	15	1
Heat production	W m^{-3}	3×10^{6}	3×10^{6}	3×10^{6}	3×10^{6}	3×10^{6}
Transmissivity	m^2 s^{-1}	7.3×10^{-5}	2.55×10^{-4}	0.4	3×10^{-4}	6.3×10^{-5}

2. Methodology

In this section, the mathematical modeling is discussed in two stages. In the first part, governing equations for cold water dynamics in the porous media is presented and in the second part a mathematical model for fluid leakage from the wellbore is discussed.

2.1 Reservoir flow modeling

A constant heat flux of 0.07 W/m² was assigned at the bottom boundary of the domain. All other exterior boundaries of the modelled domain are defined as no flow for both fluid and heat transmission. Since, the weather conditions of Soultz are not available, the monthly averaged daily weather fluctuation of Strasbourg, France was used for this study. Strasbourg is approximately 40 km SSE from the Soultz geothermal site. All fractures within the domain are regarded as internal boundaries, implicitly considering the mass

Preprints (www.preprints.org) | NOT PEER-REVIEWED | Posted: 11 October 2021 doi:10.20944/preprints202110.0169.v1

and energy exchange between porous media and fractures or fault zones. In the injection well, the diameter of the well is small and can as simplification be represented by a line.

The coupled heat and mass transfer in a fractured rock matrix can be modeled using the mass balance equation integrated with heat transport. The governing equation for heat and mass flow in porous media can be written as:

$$\rho_1(\phi_m S_1 + (1-\phi_m)S_m)\frac{\partial p}{\partial t} - \rho_1(\alpha_m(\phi_m\beta_1 + (1-\phi_m)\beta_m))\frac{\partial T}{\partial t} = \nabla.(\frac{\rho_1 k_m}{\mu}\nabla p) \qquad [1]$$

In the above equation fluid pressure and temperature in the rock matrix are denoted by p and T respectively. Here rock porosity is ϕ_m, storage coefficients for rock and fluid are S_1 and S_m. The thermal expansion coefficient of the fluid and rock matrix is denoted by β_1 and β_m respectively. The fluid density and dynamic viscosity are indicated using ρ_1 and μ whereas the reservoir permeability is denoted by k_m.

The fractures are assumed as internal boundaries and the flow along the internal fractures can be denoted by:

$$\rho_1(\phi_f S_1 + (1-\phi_f)S_{mf})e_h\frac{\partial p}{\partial t} - \rho_1(\alpha_f(\phi_f\beta_1 + (1-\phi_f)\beta_f))e_h\frac{\partial T}{\partial t} = \nabla_T.\left(\frac{e_h\rho_1 k_f}{\mu}\nabla_T p\right) + n.Q_m \qquad [2]$$

Here fluid pressure and temperature in the fracture are indicated by p and T respectively. Additionally, ϕ_f, S_f, β_f, e_h and k_f denotes the fracture porosity, storage coefficients of the fracture, thermal expansion coefficient of the fracture, hydraulic aperture between the two fracture surfaces, and fracture permeability, respectively. The mass flux exchange between the fracture and matrix are denoted by $n.Q_m = n.(-\frac{\rho k_m}{\mu \nabla p})$ whereas the gradient operator applicable along the fracture tangential plane is indicated by ∇_T.

The local thermal non-equilibrium (LTNE) approach to model heat exchange between the rock matrix and water is implemented in this study. The conductive heat transfer between rock matrix and pore fluid is the dominant heat exchange mechanism. For the rock matrix, the heat transfer equation can be written as

$$(1-\phi_m)\rho_m C_{p,m}\frac{\partial T_m}{\partial t} = \nabla.\left((1-\phi_m)\lambda_m\nabla T_m\right) + q_{ml}(T_l - T_m) \qquad [3]$$

In the above equation rock matrix and fluid temperatures are denoted by T_m and T_l, respectively. Here rock density, rock specific heat capacity, rock thermal conductivity and the rock-fluid heat transfer coefficient are denoted by ρ_m, $C_{p,m}$, λ_m and q_{ml} respectively. The heat flux leaving the domain and received by the adjacent fracture can be written as

$$(1-\phi_f)e_h\rho_f C_{p,f}\frac{\partial T_m}{\partial t} = \nabla_T.\left(\left(1-\phi_f\right)e_h\lambda_f\nabla_T T_m\right) + e_h q_{fl}(T_l - T_m) + n.(-(1-\phi_m)\lambda_m\nabla T_m) \qquad [4]$$

where T_m and T_l are the matrix and fluid temperatures in the fracture, respectively; ρ_f is the density of the fracture; $C_{p,f}$ is the specific heat capacity of the fracture; λ_f is the thermal conductivity of the fracture; and q_{fl} represents the rock fracture-fluid interface heat transfer coefficient, related to the fracture aperture. Last term on the right-hand side of the Eq. [4] represents the heat flux exchange between rock matrix and the fracture.

The heat convection equation for the pore fluid can be written as:

Preprints (www.preprints.org) | NOT PEER-REVIEWED | Posted: 11 October 2021 doi:10.20944/preprints202110.0169.v1

$$\boldsymbol{\phi_m \rho_l C_{p,l} \frac{\partial T_l}{\partial t} + \phi_m \rho_l C_{p,l} (-\frac{k_m \nabla p}{\mu}). \nabla T_l = \nabla. (\phi_m \lambda_l \nabla T_l) + q_{ml} (T_m - T_l)} \qquad [5]$$

Here $\boldsymbol{C_{p,l}}$ is the heat capacity of the fluid at a constant pressure and $\boldsymbol{\lambda_l}$ is the thermal conductivity of the fluid.

The heat flux coupling relationship of the fluid between the domain and the fracture is satisfied by:

$$\boldsymbol{\phi_f e_h \rho_l C_{p,l} \frac{\partial T_l}{\partial t} + \phi_f e_h \rho_l C_{p,l} (-\frac{k_f \nabla_T p}{\mu}). \nabla_T T_l = \nabla_T. \left(\phi_f e_h \lambda_l \nabla_T T_l\right) + e_h q_{fl} (T_m - T_l) + \ n. q_l}$$
[6]

where the heat flux $\boldsymbol{n. q_l = n. (-\phi_l \lambda_l \nabla T_l)}$ denotes the heat exchange of the fluid between porous media and the fracture.

Temperature-dependent fluid thermodynamic properties are implemented into the coupled hydrothermal mass and energy balance equations. The thermophysical properties of water as a function of temperature including dynamic viscosity ($\boldsymbol{\mu}$), specific heat capacity ($\boldsymbol{C_p}$), density ($\boldsymbol{\rho}$), and thermal diffusivity ($\boldsymbol{\kappa}$) are listed below:

$$\boldsymbol{\mu = 1.38 - 2.12 \times 10^{-2} \times T^1 + 1.36 \times 10^{-4} \times T^2 - 4.65 \times 10^{-7} \times T^3 + 8.90 \times 10^{-10} \times T^4 - 9.08 \times 10^{-13} \times T^5 + 3.85 \times 10^{-16} \times T^6 \qquad (273.15 - 413.15\ K)}$$
[7]

$$\boldsymbol{\mu = 4.01 \times 10^{-3} - 2.11 \times 10^{-5} \times T^1 + 3.86 \times 10^{-8} \times T^2 - 2.40 \times 10^{-11} \times T^3 \ (413.15 - 553.15\ K)} \qquad [8]$$

$$\boldsymbol{C_p = 1.20 \times 10^4 - 8.04 \times 10^1 \times T^1 + 3.10 \times 10^{-1} \times T^2 - 5.38 \times 10^{-4} \times T^3 + 3.63 \times 10^{-7} \times T^4} \ [12]$$

$$\boldsymbol{\rho = 1.03 \times 10^{-5} \times T^3 - 1.34 \times 10^{-2} \times T^2 + 4.97 \times T + 4.32 \times 10^2} \qquad [9]$$

$$\boldsymbol{\kappa = -8.69 \times 10^{-1} + 8.95 \times 10^{-3} \times T^1 - 1.58 \times 10^{-5} \times T^2 + 7.98 \times 10^{-9} \times T^3}$$
[10]

We have used the commercial software COMSOL Multiphysics, version 5.5 [29] for numerically solving the coupled mass and energy conservation equations listed above. COMSOL Multiphysics solves general-purpose partial differential equations using the finite element method.

2.2 Wellbore leakage modeling

Understanding the fluid flowing temperature along the wellbore can be useful for an accurate estimation of the overall heat production at the production well head temperature as well as in estimating any possible leakage caused heat loss along the wellbore. Several reliable analytical techniques are reported in literature to calculate the flowing temperature distribution along a wellbore [30-32].

Preprints (www.preprints.org) | NOT PEER-REVIEWED | Posted: 11 October 2021 doi:10.20944/preprints202110.0169.v1

We have integrated our reservoir simulation with a wellbore flow model as developed by Hasan et al. [31]. The model constitutes an analytical approach to estimate wellbore-fluid temperature distribution for steady state flow. In this method, the wellbore is split into two uniform sections for thermal properties and deviation angle. The analytical equations are solved sequentially for each section. Figure 4 shows in simplification a typical geothermal well with one deviation angle. The well is inclined at an angle α with the horizontal plane. The heat transfer between wellbore fluid and the rock matrix occurs due to temperature difference between them. A general energy balance equation for single phase fluid flow can be expressed as:

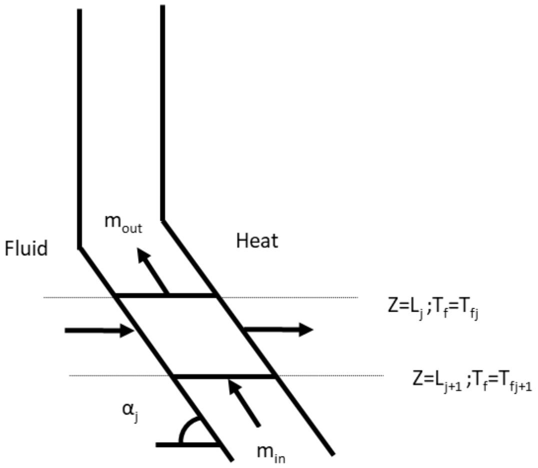

Figure 4: Wellbore heat loss modeling schematic.

$$\frac{dH}{dz} - g\ sin\alpha + v\frac{dv}{dz} = \pm\frac{Q}{w} \qquad [11]$$

Here, H is the fluid enthalpy, g is gravitational constant, z is the variable well depth from the surface, v is flow velocity, Q is the heat flux per unit of well length and w is the mass rate. When assuming no-phase change conditions, enthalpy will become:

$$dH = (\frac{\partial H}{\partial T})_p dT + (\frac{\partial H}{\partial p})_T dp = c_p dT - C_J c_p dp \qquad [12]$$

In the above equation, T is the fluid temperature and p is pressure, c_p is specific heat capacity of fluid, C_J is Joule-Thomson coefficient. If T_f is the fluid temperature, the energy balance equation will be:

$$\frac{dT_f}{dz} = C_J\frac{dp}{dz} + \frac{1}{c_p}(\pm\frac{Q}{W} + g\ sin\alpha - v\frac{dv}{dz}) \qquad [13]$$

The heat flux per unit wellbore length can be expressed as:

$$Q \equiv -L_R w c_p (T_f - T_{ei}) \qquad [14]$$

Here, T_{ei} is the rock temperature, and L_R is the relaxation parameter defined as:

$$L_R \equiv \frac{2\pi}{c_p w}[\frac{r_{to}U_{to}k_e}{\lambda_m + (r_{to}U_{to}T_D)}] \qquad [15]$$

$$T_f = T_{ei} + \frac{1-e^{(z-L)L_R}}{L_R}[g_G\ sin\alpha + \Phi - \frac{g\ sin\alpha}{c_p}] \qquad [16]$$

In Eq. (15) and (16), r_{to} is the tubing outside radius, U_{to} is the overall heat transfer coefficient, k_e is rock thermal conductivity, T_D is nondimensional temperature, L is measured depth of wellbore, g_G is the geothermal gradient. and Φ is the lumped parameter and it lumps the kinetic energy term as well as the Joule-Thomson coefficient term.

If V is the fluid specific volume and S is fluid entropy then from Maxwell identities, we can write:

$$\left(\frac{\partial H}{\partial p}\right)_T = V + T\left(\frac{\partial S}{\partial p}\right)_T \;\&\; \left(\frac{\partial S}{\partial p}\right)_T = -\left(\frac{\partial V}{\partial T}\right)_p \qquad [17]$$

$$dH = c_p dT + \left[V - T\left(\frac{\partial V}{\partial T}\right)_p\right]dp \qquad [18]$$

$$c_p C_J = -\left[V - T\left(\frac{\partial V}{\partial T}\right)_p\right] \qquad [19]$$

For liquids if ρ is the liquid density, volume expansivity (β) can be calculated as:

$$\beta \equiv \left(\frac{1}{V}\right)\left(\frac{\partial V}{\partial T}\right)_p \equiv \left(-\frac{1}{\rho}\right)\left(\frac{\partial \rho}{\partial T}\right)_p \qquad [20]$$

$$dH = c_p dT + V(1 - \beta T)dp \qquad [21]$$

$$c_p C_J = -V(1 - \beta T) \qquad [22]$$

Therefore, the final output temperature from the wellhead will be:

$$T_{out} = \frac{\int m\, c_p\, T\, dz}{\int m\, c_p\, dz} \qquad [23]$$

In this text, we considered three wells, GPK-3 and GPK-4 as two injection wells and GPK-2 as production wells. In GPK-3, the wellbore leakage was assumed between 1282 m and 4852 m depth measured from the surface. In case of GPK-2, the wellbore leakage was modeled between 1264 m to 4244 m depth measured from the surface. The fluid is single phase water flow and the model parameters are constant specific heat capacity of water as 4200 J/kg/k, $L_R = 0.00001$ 1/m and $\Phi = 0.00345$ K/m, respectively. Here L_R and Φ accounts for the casing properties, cement properties and their thicknesses.

3. Results

In this section, first the hydro-thermal numerical modelling results are compared with the operational data measured at Soultz-sous-Forêts for three years of operation. Furthermore, new injection scenarios are proposed that can be adopted with the existing industrial setup to enhance the energy extraction capability.

The operational data for three years has been made available for Soultz-Sous Forets site by the site operators and is used here to calibrate the coupled unsteady hydro-thermal model. Figure 5 shows the injection and production rates at the wellhead for 1163 days from June 2016 to September 2019. The fluid injection temperature is 70 °C for both the injection wells.

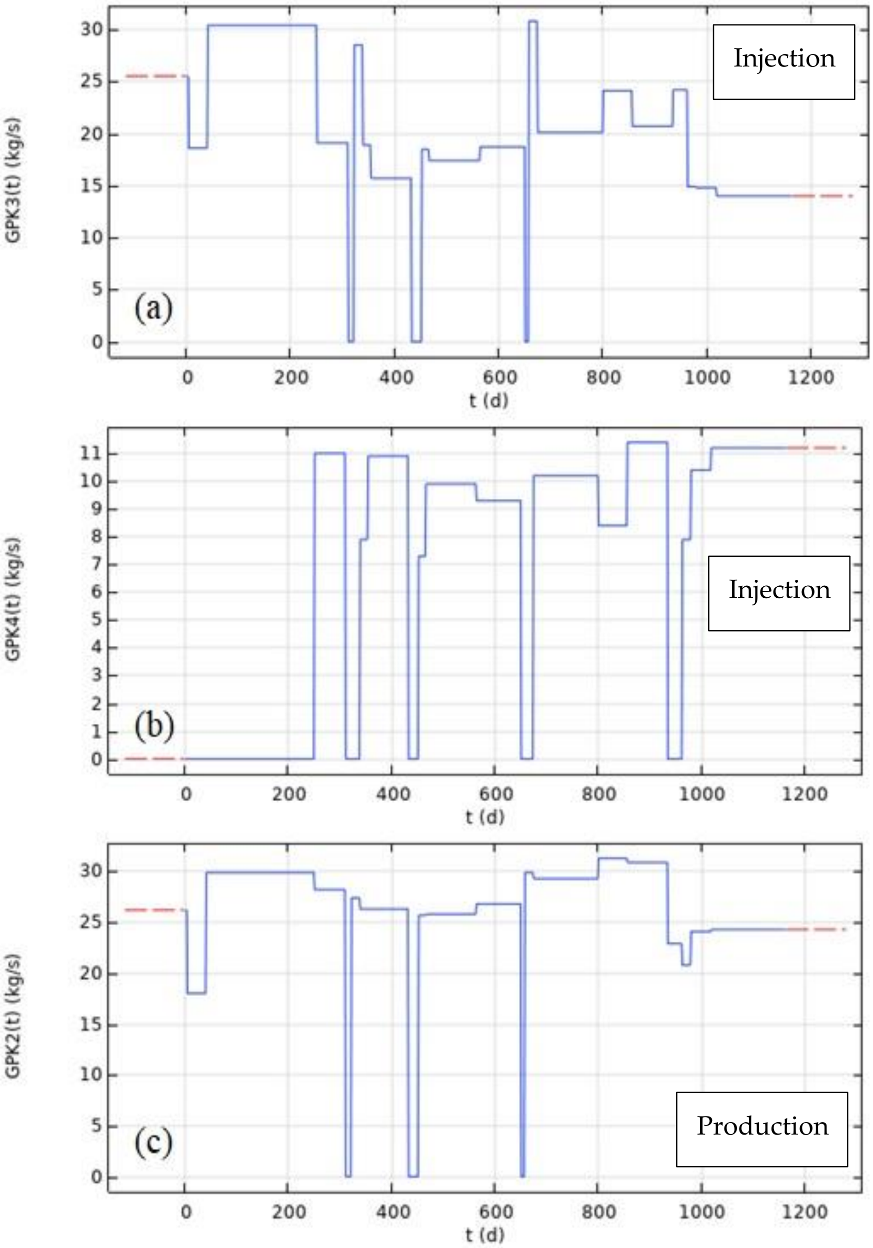

Figure 5: Injection schedule at (a) GPK-3 and (b) GPK-4 and production schedule at production well GPK-2 for 1163 days of operation from June 2016 to September 2019. Here the blue lines are the actual injection and production rates. The red dash lines indicate no operation period.

In Figure 6, the numerical model data is validated with operational data for the time period as described above. The measured temperature data is the operational data for 1163 days at the production wellhead. The temperature at the production well based on the hydro-thermal model is significantly different compared to the operational data. For most of the operational period, the predicted production well temperature is 15 ℃ higher than the measured temperature. Only operation onset and termination stages display smaller deviation in predicted temperature than observed temperature. Since the wellhead temperature measurement may get affected by the local ambient temperature and the monthly average temperature near the geothermal site is almost the same for the corresponding months in each operational year, a correction factor to account for the weather

Preprints (www.preprints.org) | NOT PEER-REVIEWED | Posted: 11 October 2021 doi:10.20944/preprints202110.0169.v1

impact on production temperature based on the numerical model was introduced. Two scenarios of seasonal impact are considered, (a) 20% impact of ambient temperature ($T_{effective}$=$T_{simulation}$ + 0.2×ambient temperature) and (b) 50 % impact of ambient temperature ($T_{effective}$ =$T_{simulation}$ + 0.5×ambient temperature) on the production fluid temperature. Figure 6 shows the comparison of the operational data with the coupled reservoir-wellbore model and weather influenced production fluid temperature. The integrated wellbore – reservoir model has the highest overestimation of production temperature. However, when daily weather fluctuation in the integrated wellbore-reservoir model are considered, the prediction matches very well for most part of the operation as shown in Figure 6. The difference between operational and numerical data while considering 50% of the ambient temperature on the production temperature of the coupled wellbore-reservoir model has the best matching among all models. However, the model deviates by more than 15 ℃ from the operation data during the period of 1.8 years and 2.4 years. Since no other reasons for these deviations are provided with the operational data set, different measurement procedures or false measurements at the wellhead are assumed as reasons for these deviations.

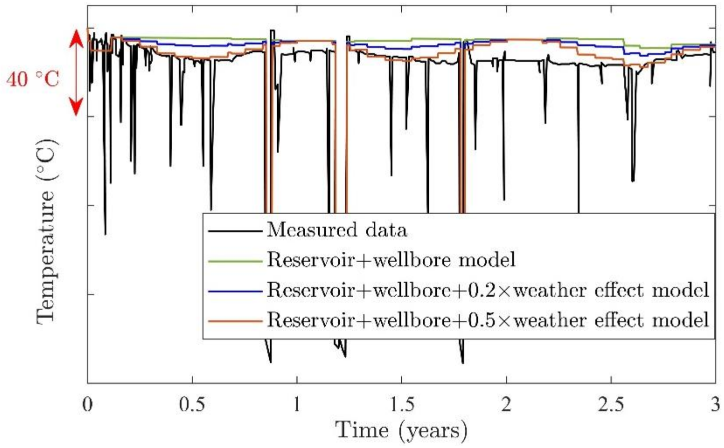

Figure 6: Qualitative difference between operational data from June 2016 to September 2019 and the data obtained from numerical model.

In the next study, the model was extended to a simulation period of 100 years of operation to predict the wellhead temperature development at the production well. In this section, different initial temperatures at the bottom hole section than the operationally measured data were used. The main objective of this study is to estimate the temperature at the production well (GPK-2) for different injection temperatures for long-term operational periods. Two scenarios were considered, A and B. In both scenarios, the injection rates for the first 1163 days are the same as in the provided operational data set. For the remaining operational period, scenario A considers four different fluid injection temperatures at the injection wellhead (70 ℃, 60 ℃, 50 ℃ and 40 ℃). The fluid injection rates are 13.3 L/s and 11 L/s for GPK-3 and GPK-4, respectively and the production fluid rate from GPK-2 is 24.3 L/s for the remaining operational period. In Scenario B, injection rate post 1163 days are 19.6 L/s and 9.7 L/s for GPK-3 and GPK-4 respectively and the production rate at GPK-2 is 29.3 L/s; the same four injection wellhead temperature as for scenario A were considered, 70 ℃, 60 ℃, 50 ℃ and 40 ℃.

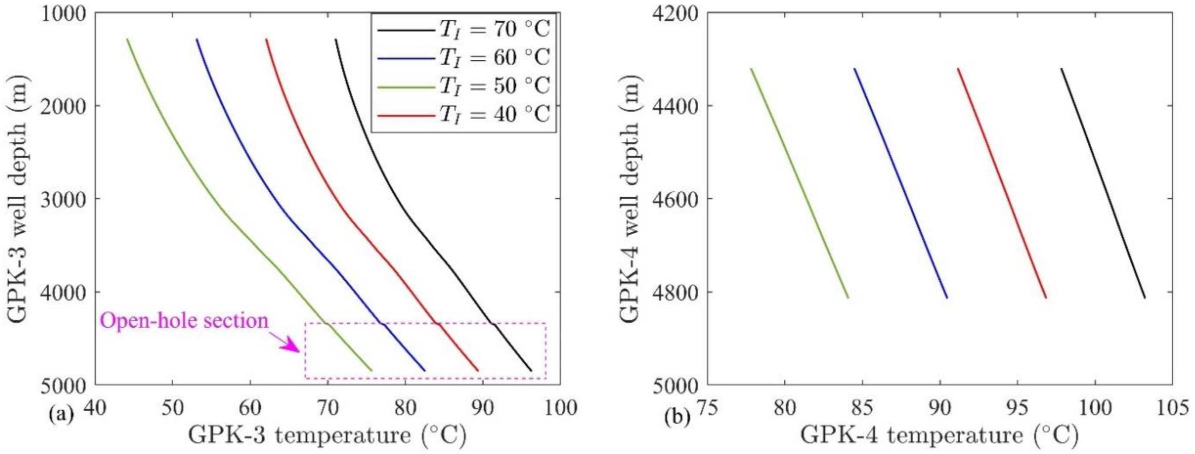

Figure 7: Temperature along the injection wells (a) GPK-3 and (b) GPK-4 with depth for Scenario A.

Figure 7 and 9 shows the temperature along the wellbore for scenario A and B respectively for both injection wells. The wellbore GPK-3 has an open hole section that causes a linear temperature drop along the wellbore instead of nonlinear temperature drop as shown in Figure 7(a) and 9(a). It is interesting to note that instead of having different injection-production rates in all three wells, the fluid production temperature at GPK-2 wellhead is almost similar for both the scenarios A and B as shown in Figure 8 and 10 respectively. The small increase in temperature at the production wellhead is due to sudden drop in the production wellhead pressure. Also, the temperature increase in scenario B is higher compared to scenario A due to the fact that scenario B has a higher production rate than scenario A which reduces the time for exchanging heat in the wellbore.

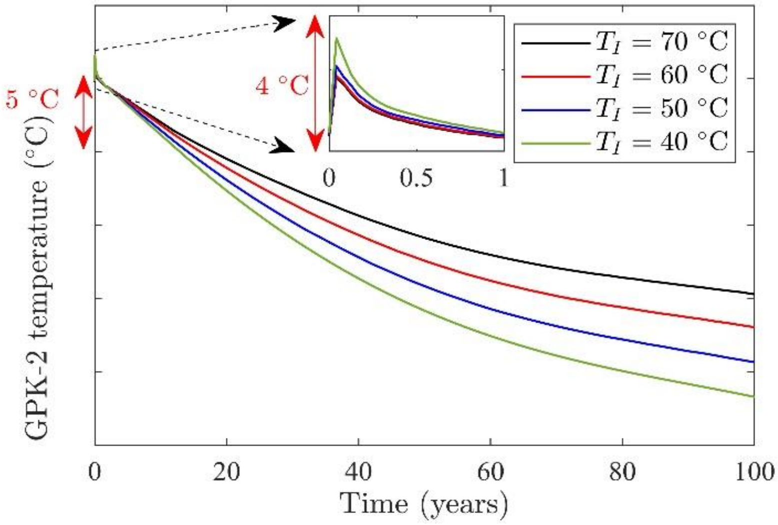

Figure 8: Wellhead temperature at the production well, GPK-2 with time for Scenario A.

Preprints (www.preprints.org) | NOT PEER-REVIEWED | Posted: 11 October 2021 doi:10.20944/preprints202110.0169.v1

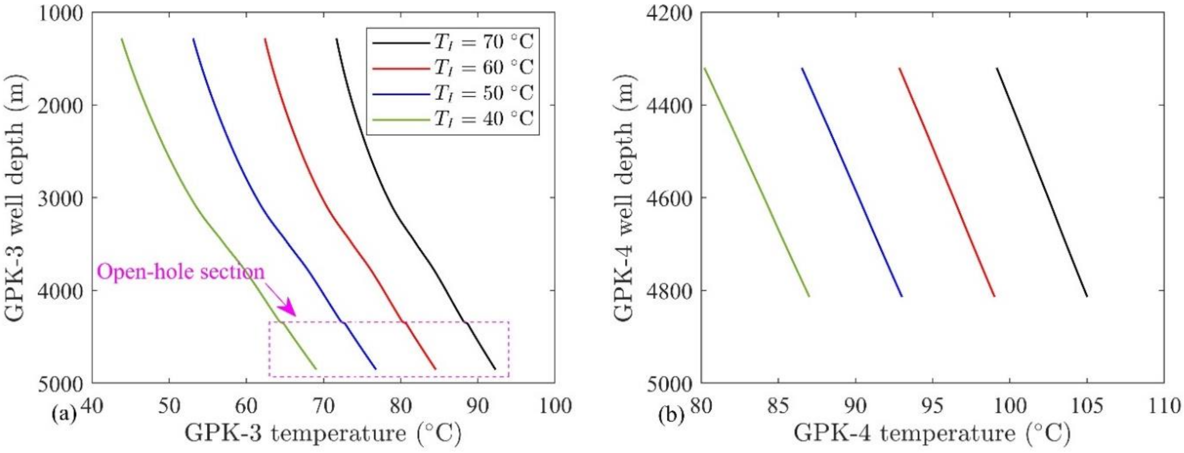

Figure 9: Temperature along the injection wells (a) GPK-3 and (b) GPK-4 with depth for Scenario B.

Figure 11 shows the comparison of temperature distribution in the fractures and along the wellbore for scenarios A and B. The higher production rate results in slightly faster thermal drawdown at the production well bottom for scenario B than scenario A. No thermal breakthrough was observed at the production well bottom even after 100 years of operation as shown in Figure 11(e & f).

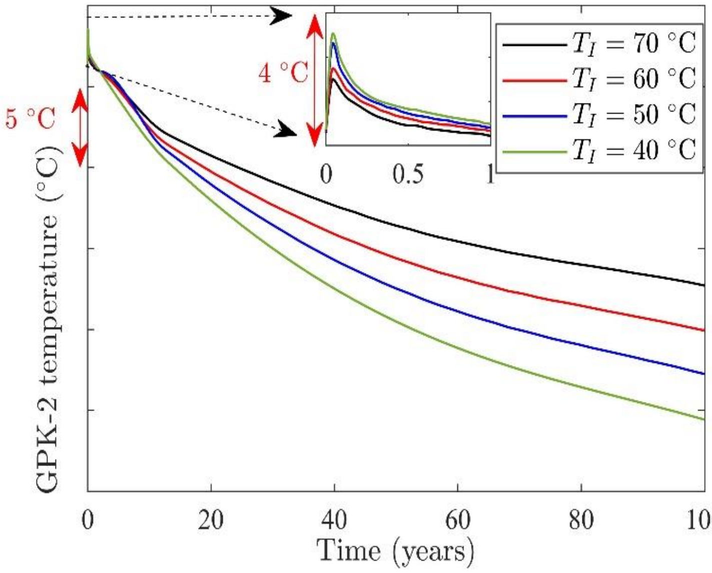

Figure 10: Wellhead temperature at the production well, GPK-2 with time for Scenario B.

5. Conclusions

As part of the MEET project, a coupled reservoir and wellbore model for hydraulic and thermal processes involved during geothermal energy extraction operation at Soultz Sous Forêts was developed. Operational data from a period of 1163 days of operation was used to validate the numerical model. The validated hydro-thermal numerical model precisely simulates the geothermal energy extraction operation for 3 years. Furthermore, two operational scenarios for 100 years with four different injection wellhead temperatures 70 ℃, 60 ℃, 50 ℃ and 40 ℃ were analyzed and it can be observed that even after 100 years of operation, thermal breakthrough at the production well is only in the range of 10 to 20°C. After 100 years of cold fluid injection and hot fluid production, the observed temperature

Preprints (www.preprints.org) | NOT PEER-REVIEWED | Posted: 11 October 2021 doi:10.20944/preprints202110.0169.v1

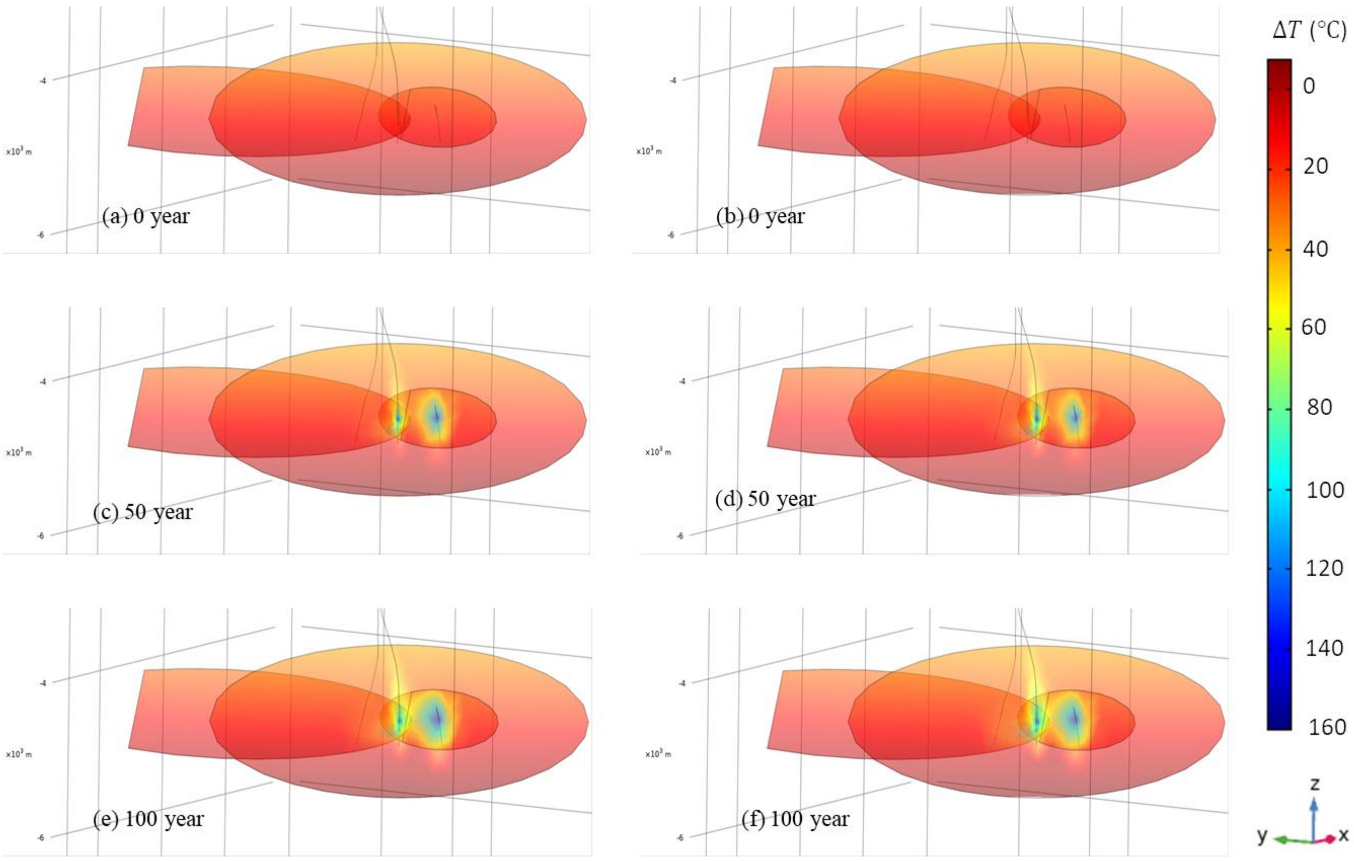

Figure 11: Comparison of temperature distribution (in SI units) in the Fractures for Scenario A and B. Here ΔT is the temperature drop in the reservoir from the initial state.

drop at the production wellhead is less than 20 ℃. Therefore, our numerical model predicts that 100 years of geothermal energy extraction operation at Soultz-sous-Forêts is feasible and will have sufficiently high production temperature throughout the operation duration.

Author Contributions: Conceptualization, S. Mahmoodpour and K. Bär.; methodology, S. Mahmoodpour and M. Singh.; software, S. Mahmoodpour and M. Singh; validation, S. Mahmoodpour and M. Singh writing—original draft preparation, S. Mahmoodpour and M. Singh; writing—review and editing, K. Bär, A. Turan.; visualization, S. Mahmoodpour and M. Singh; supervision, K- Bär and I. Sass; project administration, K. Bär; funding acquisition, K.Bär. All authors have read and agreed to the published version of the manuscript.

Funding: The work is conducted as part of the MEET project that has received funding from the European Union’s Horizon 2020 research and innovation programme under grant agreement No 792037. Authors have received support from the Group of Geothermal Science and Technology, Institute of Applied Geosciences, Technische Universität Darmstadt.

Data Availability Statement: Restrictions apply to the availability of these data. Data was obtained from [ÉS-Géothermie] and are available [https://geothermie.es.fr/en/contact/] with the permission of [ÉS-Géothermie].

Acknowledgments: Authors would like to thank ÉS-Géothermie and GEIE Exploitation de la Chaleur for providing Soultz-sous-Forêts operational data.

Conflicts of Interest: The authors declare no conflict of interest.

References

1. COP-21. Paris agreement, united nations Framework convention on climate change, conference of the parties 21, https://unfccc.int/process-and-meetings/the-paris-agreement/the-paris-agreement. France, Paris 2015, Retrieved on 15th June 2021.

Preprints (www.preprints.org) | NOT PEER-REVIEWED | Posted: 11 October 2021 doi:10.20944/preprints202110.0169.v1

2. Mahmoodpour, S.; Amooie, A.; Rostami, B.; Bahrami, F. Effect of gas impurity on the convective dissolution of CO_2 in porous media. Energy, 2020, 199, 117397.
3. Mahmoodpour, S.; Rostami, B.; Soltanian, M.R.; Amooie, A., Convective dissolution of carbon dioxide in deep saline aquifers: Insights from engineering a high-pressure porous cell. Phys. Rev. Appl., 2019, 12, 034016.
4. Singh, M.; Chaudhuri, A.; Stauffer, P.H.; Pawar, R.J.; Simulation of gravitational instability and thermo-solutal convection during the dissolution of CO2 in deep storage reservoirs Wat. Resour. Resear., 2020a, 56, e2019WR026126.
5. Singh, M.; Tangirala, S.K.; Chaudhuri, A. Potential of CO_2 based geothermal energy extraction from hot sedimentary and dry rock reservoirs, and enabling carbon geo-sequestration. Geom. Geop. Geo-Energy Geo-resour., 2020b, 6, 16.
6. Singh, M.; Chaudhuri, A.; Soltanian, M.R.; Stauffer, P.H. Coupled multiphase flow and transport simulation to model CO_2 dissolution and local capillary trapping in permeability and capillary heterogeneous reservoir. Int. J. Green. Gas. Cont., 2021, 108, 103329.
7. EGEC Geothermal. The geothermal energy market grows exponentially, but needs the right market conditions to thrive. https://www.egec.org/the-geothermal-energy-market-grows-exponentially-but-needs-the-right-market-conditions-to-thrive/, June 2020, Accessed on 15th June 2021.
8. Longa, F.D.; Nogueira, L.P.; Limberger, J.; van Wees, J.-D.; Zwaan, B. v.d.; Scenarios for geothermal energy deployment in Europe. Energy, 2020, 206, 118060.
9. Baillieux O., Schill E., Edel J.-B., Mauri G., 2013. Localization of temperature anomalies in the Upper Rhine Graben: insights from geophysics and neotectonics activity. Int. Geol. Rev. 55, 1744-1762.
10. Rolin, P.; Hehn, R.; Dalmais, E.; Genter, A. D3.3 Hydrothermal model matching colder reinjection design, WP3: Upscaling of thermal power production and optimized operation of EGS plants. 2018, H2020 Grant Agreement No-792037.
11. Duringer, P.; Aichholzer, C.; Orciani, S.; Genter, A. The Complete Lithostratigraphic Section of the Geothermal Wells in Rittershoffen (Upper Rhine Graben, Eastern France): A Key for Future Geothermal Wells. BSGF Earth Sci. Bull. 2019, 190, 13.
12. Cocherie, A.; Guerrot, C.; Fanning, C.M.; Genter, A. Datation U–Pb Des Deux Faciès Du Granite de Soultz (Fossé Rhénan, France). Comptes Rendus Geosci., 2004, 336, 775–787.
13. Schill, E.; Genter, A.; Cuenot, N.; Kohl, T. Hydraulic performance history at the Sultz EGS reservoirs from stimulation and long term circulation tests. Geothermics, 2017, 70, 110-124.
14. Vallier, B; Magnenet, V.; Schmittbuhl, J.; Fond, C. Large scale hydro-thermal circulation in the deep geothermal reservoir of Soultz-sous-Forêts. Geothermics, 2020, 78, 154-169.
15. Genter, A.; Guillou-Frottier, L.; Feybesse, J.-L.; Nicol, N.; Dezayes, C.; Schwartz, S. Typology of potential hot fractured rock resources in Europe. Geothermics, 2003, 32, 701–710.
16. Bächler, D.; Kohl, T.; Rybach, L. Impact of graben-parallel faults on hydrothermal convection—Rhine Graben case study. Physics and Chemistry of the Earth, Parts A/B/C, 2003, 28, 431–441.
17. Kohl, T.; Bächler, D.; Rybach, L. Steps towards a comprehensive thermo-hydraulic analysis of the HDR test site Soultz-sous-Forêts. In: Proceedings, World Geothermal Congress. Beppu_Morioka, Japan., 2000, pp. 2671–2676.
18. Guillou-Frottier, L.; Carre, C.; Bourgine, B.; Bouchot, V.; Genter, A. Structure of hydrothermal convection in the Upper Rhine Graben as inferred from corrected temperature data and basin-scale numerical models. J. Volcan. Geoth. Res., 2013, 256, 29-49.
19. Sausse J.; Dezayes C.; Dorbath L.; Genter A.; Place J. 3D model of fracture zones at Soultz-sous-Forêts based on geological data, image logs, induced microseismicity and vertical seismic profiles. C. R. Geoscience, 2010, 342, 531-545, https://doi.org/10.1016/j.crte.2010.01.011.
20. Dezayes, C.; Genter, A.; Valley, B. Structure of the low permeable naturally fractured geothermal reservoir at Soultz. C. R. Geoscience, 2010, 342, 517–530. https://doi.org/10.1016/j.crte.2009.10.002.
21. Gérard, A.; Genter, A.; Kohl, T.; Lutz, P.; Rose, P.; Rummel, F. The deep EGS (enhanced geothermal system) project at soultz-sous-Forêts (Alsace, France). Geothermics, 2006, 35, 473–483.
22. Sanjuan, B.; Pinault, J.L.; Rose, P.; Gerard, A.; Brach, M.; Braibant, G.; Crouzet, C.; Foucher, J.C.; Gautier, A. Geochemical fluid char-acteristics and main achievements about traces tests at Soultz-sous-Forêts (France). EHDRA Scientific Conference 2006, Soultz-sous-Forêts, France; 2006.
23. Blumenthal, M.; Kuhn, M.; Pape, H.; Rath, V.; Clauser, C. Hydraulic model of the deep reservoir quantifying the multi-well tracer test. Proceedings of the EHDRA scientific conference, Soultz-sous-Forêts, France, 28-29 June 2007, (2007).
24. Gessner, K.; Kuhn, M.; Rath, V.; Kosack, C.; Blumenthal, M.; Clauser, C. Coupled process models as a tool for analysing hydrothermal systems. Surveys in Geophysics, 2009, 30.
25. Egert, R.; Maziar, G.K.; Held, S.; Kohl, T. Implications on large-scale flow of the fractured EGS reservoir Soultz inferred from hydraulic data and tracer experiments. Geothermics, 2020, 84, 101749.
26. Gentier, S.; Rachez, X.; Ngoc, T. D. T.; Peter-Borie, M.; Souque, C. 3D flow modelling of the medium-term circulation test performed in the deep geothermal site of Soultz-sous-Forêts (France). 2010.
27. Magnenet, V.; Fond, C.; Genter, A.; Schmittbuhl, J. Two-dimensional THM modelling of the large scale natural hydrothermal circulation at Soultz-sous-Forêts. Geothermal Energy, 2014, https://link.springer.com/article/10.1186/s40517-014-0017-x.

Preprints (www.preprints.org) | NOT PEER-REVIEWED | Posted: 11 October 2021 doi:10.20944/preprints202110.0169.v1

28. Aliyu, M. D.; Chen H. Numerical modelling of coupled hydro-thermal processes of the Soultz heterogeneous geothermal system. in Seventh European Congress on Computational Methods in Applied Sciences and Engineering ECCOMAS Congress Stanford University, Crete Island, Greece, June 05-10, 2016.
29. COMSOL Multiphysics® v. 5.5. www.comsol.com. COMSOL AB, Stockholm, Sweden.
30. Alves, I.N.; Alhanatl, F.J.S.; Shoham, O. A unified model for predicting flowing temperature distribution in wellbores and pipelines. SPE Prod. Engg, November 1992, 363-367.
31. Hasan, A.R.; Kabir, C.S.; Wang, X. A robust steady-state model for flowing fluid temperature in complex wells. SPE Prod. Operat., May 2009, 269-276.
32. Moradi, B.; Ayoub, M.; Bataee, M.; Mohammadian, E. Calculation of temperature profile in injection wells. J. Pet. Explor. Prod. Tec., 2020, 10, 687-697.